Decoding Liquid Crystal Oligomer Phase Transitions: Towards Molecularly-Engineered Shape Changing Materials

Journal:	*Macromolecules*
Manuscript ID	ma-2019-01218v.R1
Manuscript Type:	Article
Date Submitted by the Author:	13-Aug-2019
Complete List of Authors:	Guo, Yuanhang; Pusan National University, Polymer Science and Engineering Lee, Jieun; Pusan National University, Polymer Science and Engineering Son, Jinha; Pusan National University, Polymer Science and Engineering Ahn, Suk-Kyun; Pusan National University, Polymer Science and Engineering Carrillo, Jan-Michael; Oak Ridge National Laboratory, Sumpter, Bobby; Oak Ridge National Laboratory, Computer Science and Mathematics Division

Decoding Liquid Crystal Oligomer Phase Transitions: Towards Molecularly-Engineered Shape Changing Materials

Yuanhang Guo,[1] Jieun Lee,[1] Jinha Son,[1] Suk-kyun Ahn,[1]* Jan-Michal Y. Carrillo,[2,3]* and Bobby G. Sumpter[2,3]

[1]Department of Polymer Science and Engineering, Pusan National University, Busan, Korea 46241

[2]Center for Nanophase Materials Sciences, Oak Ridge National Laboratory, Oak Ridge, Tennessee 37831, United States

[3]Computational Sciences and Engineering Division, Oak Ridge National Laboratory, Oak Ridge, Tennessee 37831, United States

ABSTRACT

This work details an integrated investigation of liquid crystal (LC) oligomers that combines experiments and molecular dynamics simulations for obtaining a detailed understanding of the molecular structure of LC oligomers and the mechanism underlying their phase transition temperatures. We synthesized and characterized a series of LC oligomers prepared from different lengths of methylene spacers in the reactive LC monomers and *n*-alkylamine chain extenders *via aza*-Michael addition reaction. In parallel, we performed isothermal-isobaric (NPT) ensemble coarse-grained molecular dynamics (CG-MD) simulation of analogue mesogens that are connected to flexible spacers and extenders at varying temperature, spacer length and extender length. This approach allowed the effect of length in the flexible spacer as well as in the chain extender on the nematic-isotropic transition temperature (T_{ni}) to be determined. The results showed that increasing the length of the extender decreases T_{ni} for LC oligomers and amplifies the decrease of T_{ni} in LC oligomers when the spacer length is short. We infer that the combination of spacer and extender changes the shape anisotropy of LC oligomers, changing packing behavior of constituent mesogens, thus affecting their ability to transition from the isotropic to the nematic phase. The detailed molecular structure-property relationships formulated enable prescribing design rules for LC oligomers geared towards molecularly-engineered shape changing materials.

INTRODUCTION

Liquid crystal elastomers (LCEs) are mechanically responsive materials which can undergo shape transformation in a programmed and reversible manner when exposed to external stimuli.[1-4] The ability to control LC orientation spatially and hierarchically with various methods including surface, mechanical and magnetic alignments allows for creation of 3D anisotropic shape changing materials.[5-7] Various types of soft actuators in macro-,[8-14] micro-[15-24], microarray[25-33] and surface level[34-41] have been reported by exploiting the shape programmability, elastic property and stimuli-sensitivity of LCEs. While the importance of alignment cannot be overemphasized, the materials chemistry to prepare LCEs also plays a pivotal role that can determine intrinsic properties including phase behavior, thermal and mechanical properties. Classically, the hydrosilylation chemistry in which a vinyl-functionalized LC monomer and a multifunctional vinyl crosslinker are grafted on polyhydrosiloxane main chain, producing a side-chain LCE, has been widely exploited.[11,42] This chemistry can be also applicable to prepare main-chain LCEs by reacting a divinyl LC monomer with a disiloxane chain extender and a tetrasiloxane cross-linker.[43-46] More recent studies on the LCE synthesis witness extensive use of the nematic diacrylate monomers (so-called reactive mesogens) as a building block partly because they are not only commercially available, but also can be easily aligned. Based on these versatile LC monomers, several research groups have developed various synthetic methods to prepare LCEs including *aza*-Michael addition,[8,10,47,48] *thiol*-Michael addition,[33,49-58] trans-esterification[59-61] as well as chain-transfer process.[62]

For the LCEs prepared by step-growth reaction such as the Michael addition, the characteristics and properties of LC oligomers (*i.e.*, LCE precursors) is one of the crucial factors in determining properties of resulting LCEs. For example, the crosslink density and mechanical properties will be greatly affected by molecular weight of LC oligomers.[47,48] The actuation temperature of the LCEs is related to the nematic-isotropic temperature (T_{ni}) of LC oligomers.[52,55, 63] Very recently, LC oligomers have been utilized as LC inks for the direct ink writing (DIW)-based 3D printing process. The subsequent photo-crosslinking of the patterned LC ink structures produces 2D or 3D patterned LCEs which successfully demonstrate as a new class of 4D printing materials.[52,64-66] Thus, a fundamental understanding of the impact of the molecular structure of LC oligomers on its phase behaviors and thermal properties will be crucial for proper design of LCEs and for tailoring their performance.

In this study, the phase behavior and thermal properties of a series of LC oligomers are investigated by combining experiments and coarse-grained molecular dynamics (CG-MD) simulations to reveal the molecular structure-property relationships. As a model system, poly(*β*-amino ester) types LC oligomers are synthesized by step-growth polymerization through *aza*-Michael addition reaction between diacrylate LC monomers and primary amines. In particular, the number of flexible methylene spacer in the LC monomers as well as the number of methylene group in the primary alkylamine are varied which allows for a systematic study on the phase behavior of LC oligomers. According to the CG-MD results, the shape anisotropy of the LC oligomers is greatly altered depending on the molecular structure of LC oligomers, and found to be a key parameter that changes the T_{ni}. To our knowledge, this is the first investigation of poly(*β*-amino ester) types LC oligomers that combines experiments and CG-MD simulations to obtain detailed understanding of the molecular structure of LC oligomers and their phase transition temperatures. Our study provides useful guidelines to rationally design and manipulate properties of LC oligomers geared towards molecularly-engineered shape changing materials.

EXPERIMENTAL

Materials

1,4-Bis-[4-(3-acryloyloxypropyloxy)benzoyloxy]-2-methylbenzene (LC monomer with three methylene spacer), 1,4-bis-[4-(6-acryloyloxyhexyloxy)benzoyloxy]-2-methylbenzene (LC monomer with six methylene spacer), and 1,4-bis-[4-(11-acryloyloxyundecyloxy)benzoyloxy]-2-methylbenzene (LC monomer with eleven methylene spacer), were purchased from Synthon Chemicals. *n*-butylamine, *n*-hexylamine, *n*-octylamine and *n*-decylamine were purchased from Acros. All materials were used without purification.

Synthesis of liquid crystal oligomers

In a representative synthesis, 1,4-bis-[4-(3-acryloyloxypropyloxy)benzoyloxy]-2-methylbenzene (LC monomer) and *n*-butyl amine with a molar ratio of diacrylate : primary amine = 1.1 : 1, were added to a 6 mL vial. The LC mixture was heated by a heat gun and vigorously vortexed for uniform mixing. Afterwards, the vial containing LC mixture was placed in an oven at 90 °C about 24 h, during which *aza*-Michael addition reaction proceeds between LC monomer and amine. A similar procedure was performed to synthesize other LC oligomers.

Methods and Characterizations

^{1}H NMR spectra was collected using 500 MHz Varian spectrophotometer using deuterated chloroform as solvent. Size exclusion chromatography (SEC) was performed using an Agilent 1100 pump, a refractive index detector, and PSS SDV (5 μm; 10^5, 10^3, and 10^2 Å; 8.0 × 300.0 mm) columns. THF was used as eluent, and Agilent GPC-addon (Rev. B. 01. 01) software was used to construct a conventional calibration curve using polystyrene standards. Polarizing optical microscope (POM, Nikon Eclipse LV100N POL) equipped with a heating stage (Linkam LTS420) was used to determine phase transitions of the LC oligomers using the Toupview software. T_{ni} of the LC monomers and LC oligomers were determined by cooling samples from the isotropic phase. Differential scanning calorimetry (DSC) was performed on TA instruments Q20 under nitrogen flow. The samples were heated to 150 °C, then cooled to -50 °C, and reheated to 150 °C at the rate of 10 °C/min.

SIMULATION METHOD

There are many ways to model liquid crystals, which includes both theoretical and computational studies of liquid crystals and their phase transitions,[67-77] however we opted to use coarse-grained bead-spring model of LC oligomers, since it is easier to incorporate both rigid mesogens and flexible chain spacers and extenders in the model. In this approach, in contrast to an all-atom model, the T_{ni} can be determined within the time-scale of the simulations, while preserving the particle-based nature of the simulation. Here, CG-MD simulation of LC monomers, in the isothermal-isobaric ensemble (NPT), was performed to determine the dependence of T_{ni} on the length of the mesogen spacer (N_L) and the alkylamine extender (N_D). In the CG-MD, a mesogen is represented as five connected Lennard-Jones (LJ) beads that are made rigid by the addition of a bending potential to two consecutive bonds, while the spacers and extenders are represented as flexible chains of up to 3 connected LJ beads. A monomer is represented as a set of one mesogen connected to two spacers that are each connected at the ends of the mesogen (see Figure 1b and Figure S1). The length of the alkyl spacer and the attached alkylamine extender are represented as N_L and N_D, respectively. The alignment of mesogens was monitored by examining the change of behavior and oscillations of the orientational correlation function, $g_2(r)$,[78] and the temperature at which the system transitions from the nematic to isotropic phase was recorded. The procedure for determining the T_{ni} through $g_2(r)$ are described in the Supporting Information and illustrated in Figure S2. We opted to use $g_2(r)$ to clearly see the onset of phase transition during the case

when there are multiple domains with different nematic directors, for example as seen in T=0.99 in Figure S2(a), where the value of the nematic order parameter, $\langle S_2 \rangle$,[76, 79] of the simulation box would be low. However, we also used $\langle S_2 \rangle$ and the total number density $\langle \rho \rangle$ as checks to confirm the T_{ni} as shown in Figure S2(b-c). It is expected that $\langle \rho \rangle$ would increase in the nematic phase as the mesogens are better packed than in the isotropic phase. Note, the strength of the pair-wise interactions between all Lennard-Jones beads is equal to 1 k_BT, signifying that all interactions are neutral, and the study focuses only on the entropic effect of the length of spacers and extenders on T_{ni}. Hence, the effects of these moieties to enthalpic interactions of the system, such as π-π interactions found in the phenyl rings of the mesogens were neglected. Furthermore, three mesogens are attached at their spacers through a junction bead, where the junction bead is also attached to the extender chains, to form a trimer. Similar to the simulation protocol used in simulating monomers, simulations were performed to monintor T_{ni} as a function N_L and N_D for the trimer. Also, we observe that the isotropic-nematic phase transition of the LC mesogens is first-order as indicated by the abrupt change in the behavior of $g_2(r)$, and in the values of $\langle S_2 \rangle$, and $\langle \rho \rangle$ as shown in Figure S2. All simulations were run using LAMMPS[80,81] software package with three runs having different initial configurations. More details describing the simulation protocol and simulation system sizes (see Table S1) are provided in the Supporting Information.

RESULTS AND DISCUSSION

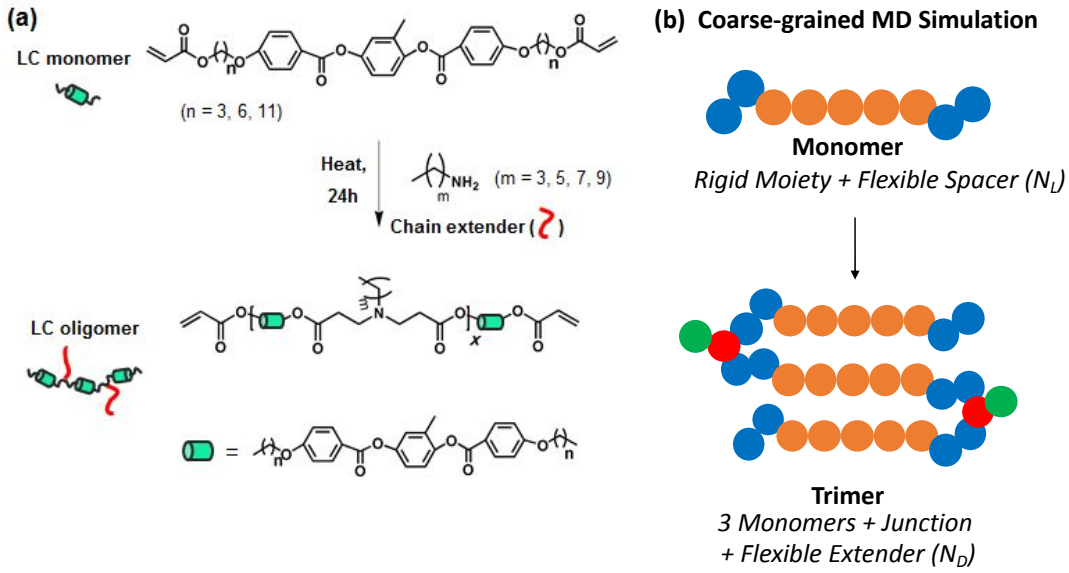

Figure 1. (a) Reaction scheme of LC oligomers by chain extending the LC monomer *via aza*-Michael addition reaction. (b) Coarse-grained representation of the monomer and the trimer where the rigid moieties in the mesogens are represented as five linked orange beads. The flexible spacers with different length (N_L) are the blue beads. The junction beads that connect the spacers are the red beads. And, the extender chain with different length (N_D) that represents the *n*-alkylamine moiety in the experiments, are the green beads.

To investigate the impact of spacer length in the LC monomers as well as the chain extenders on the resulting phase transitions of LC oligomers, in particular with T_{ni}, a series of LC oligomers were prepared. Specifically, twelve LC oligomers were synthesized by *aza*-Michael addition reaction between three LC monomers containing different length of methylene spacer (*n* = 3, 6 and 11) and various types of alkylamine chain extenders (CH_3-$(CH_2)_m$-NH_2, *m* = 3, 5, 7 and 9) as shown in Figure 1a. The synthetic protocol of the LC oligomer is similar to a previously reported method.[8,10,47] Briefly, the LC monomer and primary amine are homogeneously mixed in a vial and then oligomerized at 90 °C for 24 h. During this period, the diacrylate functionalized LC monomer is chain extended by reacting with a primary amine through step-growth polymerization, producing the poly(*β*–amino ester) type LC oligomer. The molar ratio of diacrylate in the LC monomer to primary amine in the feed is approximately 1.1:1. Throughout this article, we refer to the LC monomers consisting

of different spacer length as LCM(*n*), and LC oligomers as LCO(*n*-*m*), where *n* and *m* represent the number of methylene groups in the flexible spacer in the LC monomers and amine chain extenders, respectively. Note that the values of *n* and *m* in the experiments are analogous to N_L and N_D in the CG-MD simulations, respectively in Figure 1b.

Molecular characterizations of LC oligomers are performed using ^{1}H NMR and the representative ^{1}H NMR spectrum of LCO(3-5) with its peak assignment is shown in Figure 2. For reference, ^{1}H NMR spectra of the starting materials (LCM(3) and *n*-hexyl amine) are also shown in Figure S3. The appearance of two peaks, **l** (2.77 ppm, O(C=O)-CH_2-CH_2-NR_2-) and **n** (2.39 ppm, -C_5H_{11}CH_2-NR_2-), next to tertiary amine as well as the peak, **m** (2.45 ppm, O(C=O)-CH_2-CH_2-NR_2-) next to ester suggest the successful formation of *β*–amino ester linkage in the LC oligomers. The degree of polymerization (DP) and the number average molecular weight (M_n) are determined by the end-group analysis. Specifically, the ratio between six protons in the diacrylate end-groups (**b**, **c** and **d**) and four aromatic protons in the repeating mesogen (**a**) are used to calculate DP and M_n of each LC oligomer, and the values are summarized in Table 1. More calculation details are described in the Supporting Information, and the rest of ^{1}H NMR spectra of LC oligomers are also shown in Figure S4. We note that LC oligomers having comparable DP are prepared so that the phase behavior dependence on the molecular structure of LC oligomers rather than molecular weight of LC oligomers can be investigated.[82, 83]

The number and weight average molecular weights (M_n and M_w) of LC oligomers and their molecular weight distributions are further determined by SEC, and the values are listed in Table 1. In general, the SEC traces are broad, and multiple peaks appear especially in the high retention time, suggesting the presence of shorter LC oligomers probably due to incomplete reaction (Figure 3). As a result, broad molecular weight distributions ($Đ \sim 1.5$-2.7) are found because of the characteristics of step-growth polymerization as well as the inefficient mixing during the melt polymerization. The values of M_n determined by ^{1}H NMR and SEC tend to increase with increasing the length of spacer and chain extender.

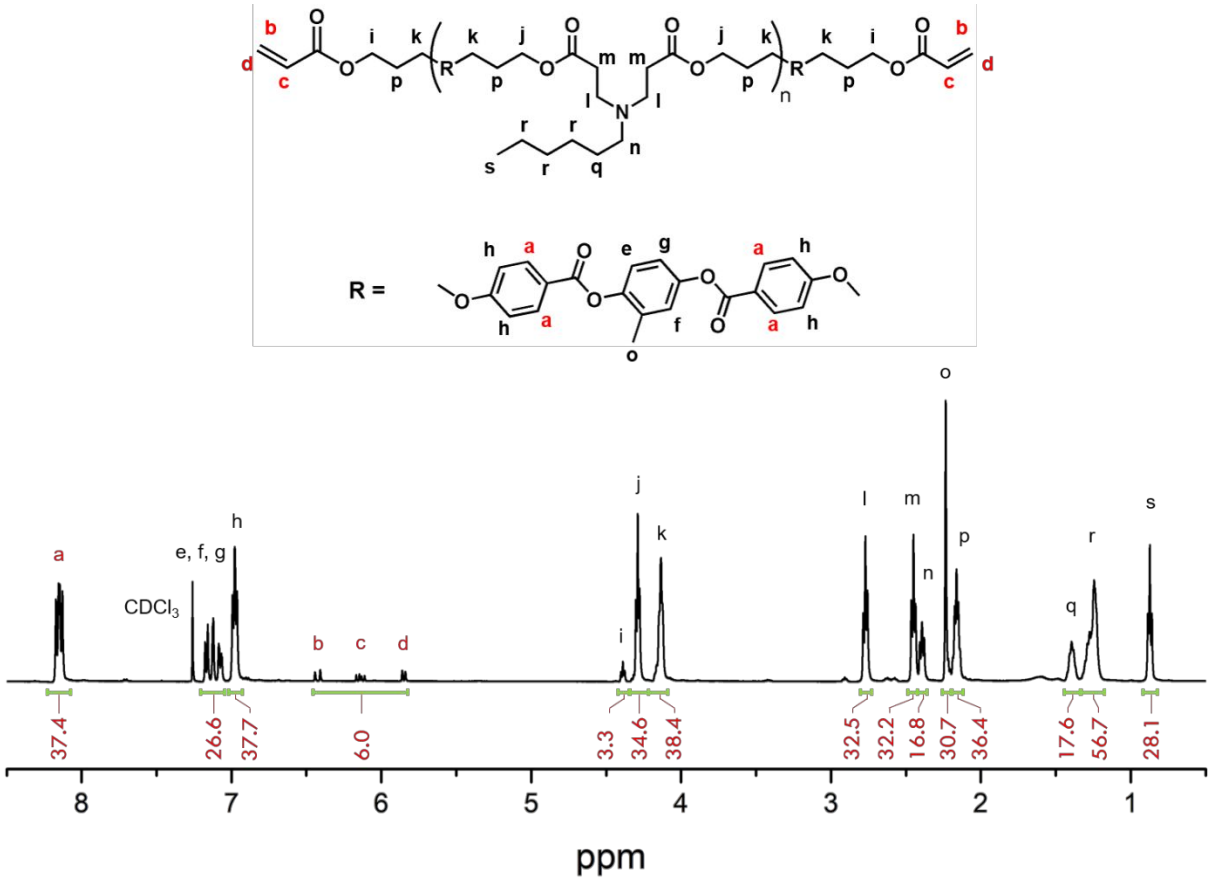

Figure 2. ^{1}H NMR spectrum of LCO(3-5) in $CDCl_3$.

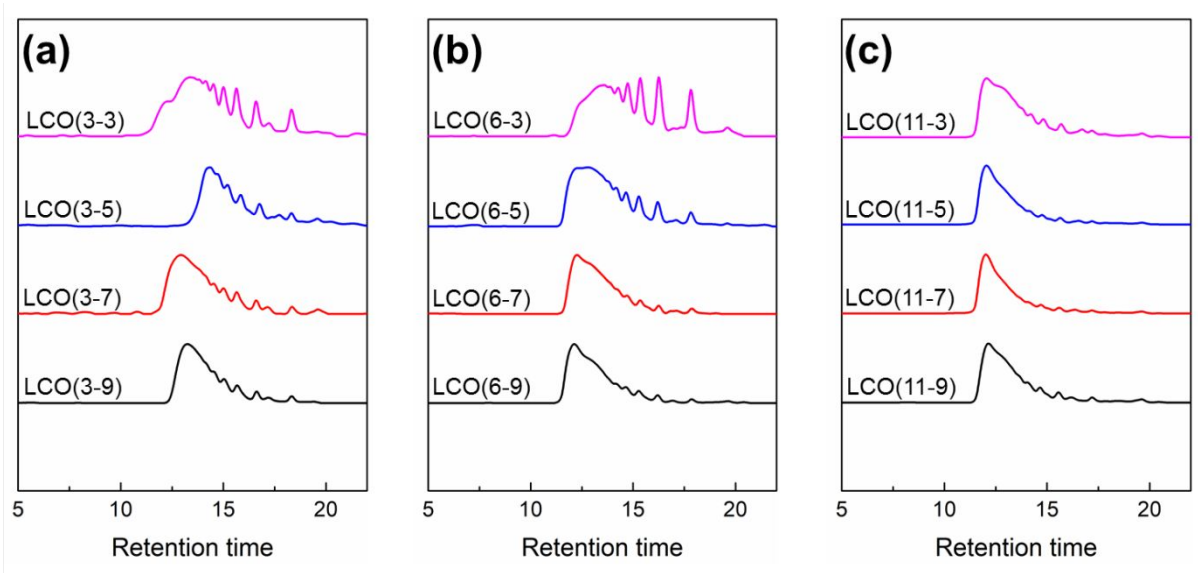

Figure 3. SEC traces collected from RI detector of LC oligomers. (a) LCO(3-*m*) series, (b) LCO(6-*m*) series and (c) LCO(11-*m*) series.

TABLE 1. Summary of molecular characterization of LC oligomers

sample	^{1}H NMR		SEC		
	DP[a]	$M_{n,\ NMR}$ (g/mol)[a]	$M_{n,SEC}$ (g/mol)[b]	$M_{w,SEC}$ (g/mol)[b]	$Đ$[b]
LCO(3-3)	6.4	4,800	4,600	12,500	2.7
LCO(3-5)	8.4	6,400	3,300	4,900	1.5
LCO(3-7)	6.9	5,500	5,000	11,800	2.4
LCO(3-9)	6.9	5,700	5,600	9,300	1.7
LCO(6-3)	8.4	6,900	5,800	10,000	1.7
LCO(6-5)	7.1	6,200	7,000	16,800	2.4
LCO(6-7)	7.7	6,800	8,500	17,400	2.0
LCO(6-9)	8.1	7,400	10,000	21,500	2.1
LCO(11-3)	9.8	9,500	9,000	20,600	2.3
LCO(11-5)	8.1	8,200	12,100	24,400	2.0
LCO(11-7)	8.6	8,900	12,100	25,700	2.1
LCO(11-9)	7.0	7,600	10,800	20,900	1.9

[a]Determined by ^{1}H NMR end-group analyses. [b]Determined by refractive index detector with PS standards in THF.

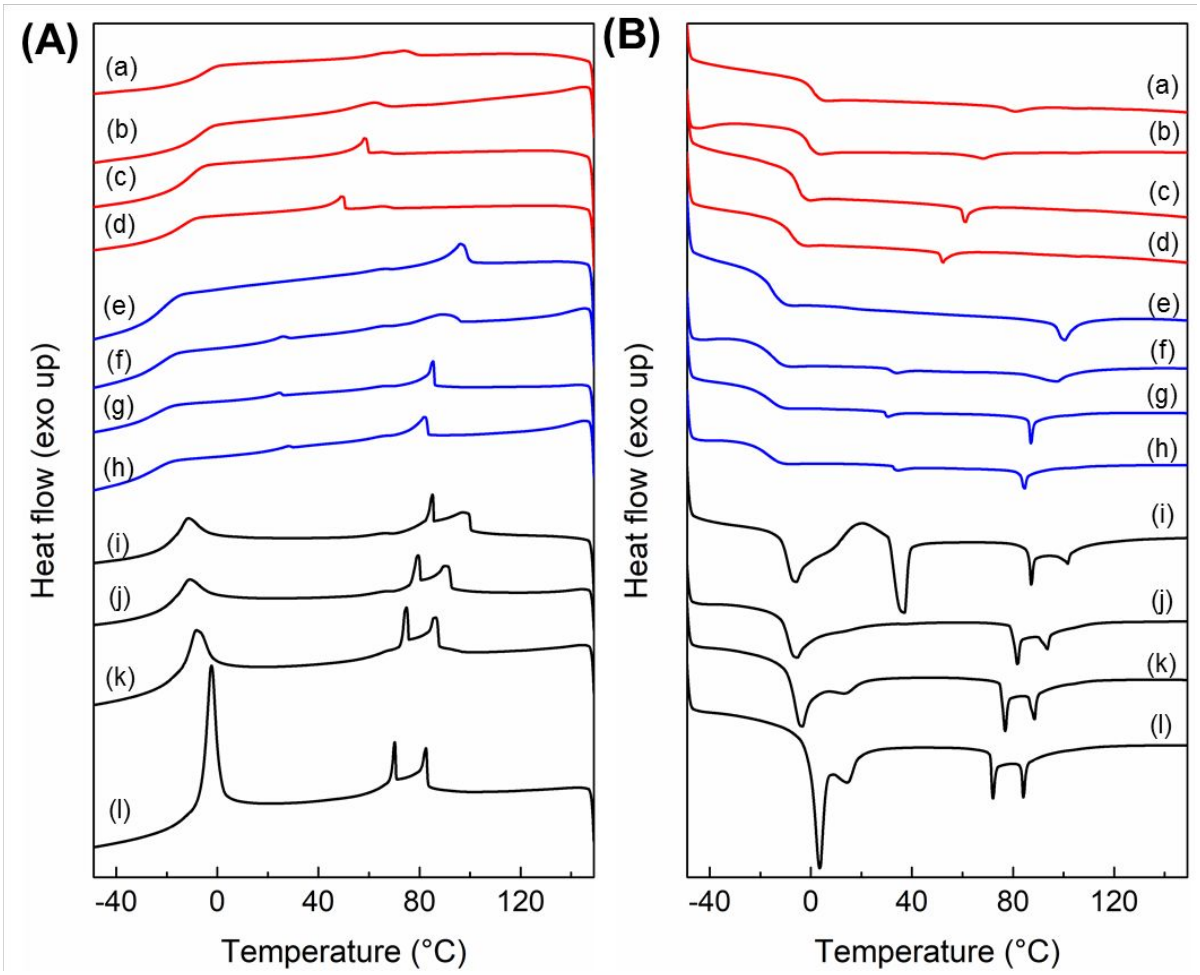

Figure 4. DSC traces of LC oligomers prepared by different types of spacer and chain-extender during (A) first cooling curves and (B) second heating curves. (a) LCO(3-3), (b) LCO(3-5), (c) LCO(3-7), (d) LCO(3-9), (e) LCO(6-3), (f) LCO(6-5), (g) LCO(6-7), (h) LCO(6-9), (i) LCO(11-3), (j) LCO(11-5), (k) LCO(11-7) and (l) LCO(11-9).

The phase transitions and thermal properties of LC monomers and LC oligomers were investigated by DSC as well as POM with temperature control. DSC traces of LC monomers and LC oligomers are shown in Figure S5 and Figure 4, and the transition temperatures and associated enthalpy changes are listed in Table S2. LC monomers show T_m and T_{ni}, and their values are close with literature.[6,84] The T_{ni} of LC monomers gradually decreases with increasing the length of the flexible methylene spacer.[84] A similar behavior is observed in the CG-MD simulations where T_{ni} in LC monomers decreases as N_L increases (See Table 2 and Figure S7b).

LC oligomers exhibit considerably different phase behaviors depending on the length of spacer in LC monomers. On one hand, LC oligomers prepared from LCM(3) and LCM(6) show a glass transition (T_g) and a LC clearing temperature. The Schlieren textures are observed for both LCO(3) and LCO(6) series, when cooling from the isotropic phase, indicating the nematic phase in these samples (Figure 5). We note that weakly noticeable peaks for LCO(6) series are detected around 31-34 ^oC in DSC traces which may imply the existence of another mesophase. However, no significant change in texture of mesophase is observed when monitored by POM even after fine temperature control. Interestingly, both T_g and T_{ni} of LCO(3) and LCO(6) series gradually decrease with increasing the length of methylene group in the amine chain extender. The reduction in T_g is associated with increase in free volume in the LC oligomers, and the suppression in T_{ni} is attributed to the destabilization of nematic phase by the longer alkyl group, which is the non-mesogenic segment.[10] It is worth noting that the LCO(3) series showed substantially lower T_{ni} than the LCO(6) series when prepared by the same type of amine chain extender, although the T_{ni} of LC monomer is higher for the LCM(3) compared to the LCM(6). Such difference between LCO(3) and LCO(6) series will be discussed in more detail later.

On the other hand, more complex phase behaviors are observed for LCO(11) series, including multiple mesophases and melting/crystallization temperature. When cooling from the isotropic phase, LCO(11) series first undergo phase transition to nematic phase, then to smectic phase and lastly to crystalline phase. The representative LC textures observed for LCO(11) series by POM at nematic phase are shown in Figure 5, and smectic and crystalline phases are shown in Figure S6. The emergence of smectic phase is probably caused by the long methylene spacer which enhance the ordering between mesogens.[55,84] During subsequent heating, the crystals of LCO(11) melt at two discrete temperature ranges of which temperature distance and associated enthalpy changes vary depending on types of chain extender employed. Both mesophase transitions (*i.e.*, nematic-isotropic and smectic-nematic) show a gradual decrease with increasing the length of methylene group in the chain extender, similar to LCO(3) and LCO(6) series.

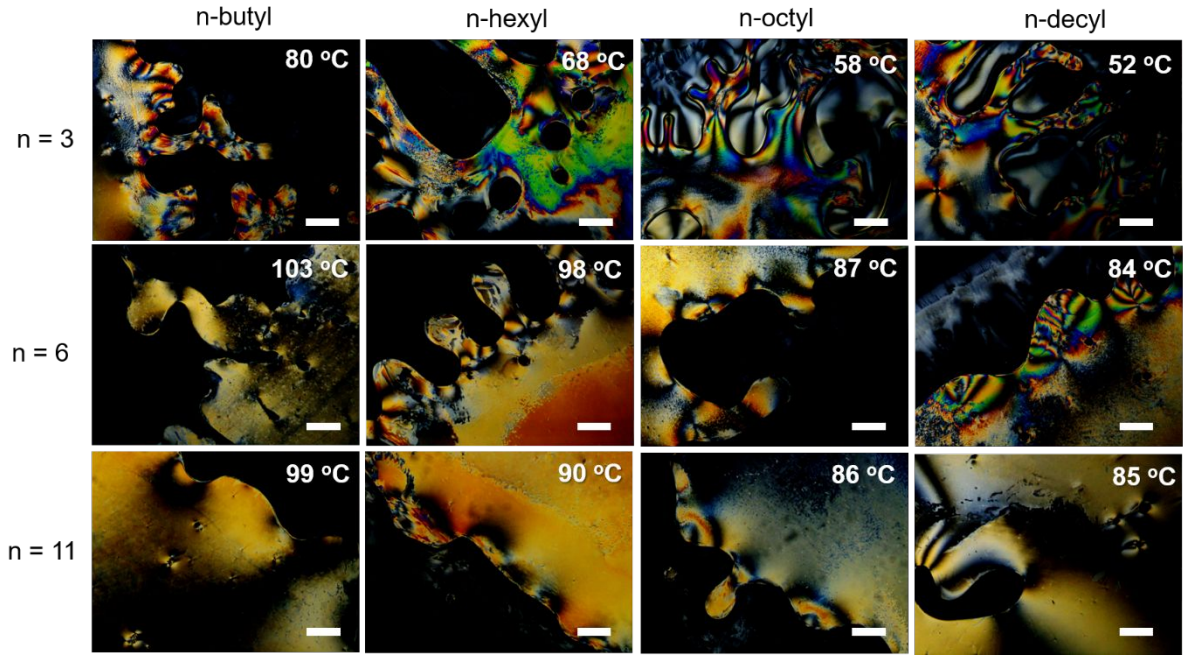

Figure 5. POM images of representative nematic textures of LC oligomers consisting of different lengths of spacer and chain-extender. Images were taken under cross polarizers and scale bars represent 100 μm.

The aim of our study is to reveal the relationship between the molecular structure of LC oligomer and the corresponding nematic-isotropic transition where the order parameter changes the most dramatically. Therefore, we mainly focus on how the T_{ni} is altered with variation in molecular structure of LC oligomers, in spite of observing multiple phase transitions in some LC oligomers. In this regard, the T_{ni} as well as the ratio of $T_{ni,oligomer}/T_{ni,monomer}$ of LC monomers and LC oligomers determined by simulation and experiment are summarized in Table 2 and Table 3, respectively. These results show several trends regarding T_{ni} change. First, LC oligomers always show lower T_{ni} than their corresponding LC monomers. Second, T_{ni} of LC oligomers gradually decreases with increasing the length of methylene group in chain extender. Similar trends of T_{ni} when considering monomers versus trimers, and dependence of N_D are seen in simulations as well. However, the experimental and simulation results show a discrepancy with respect to T_{ni} of LC oligomers at varying spacer length as shown in Figure S7. Specifically, when the same type of chain extender is employed, the LCO(3) series (*i.e.*, the shortest spacer length) show the lowest T_{ni} in the experimental results. In contrast, the trimers with N_L=3 show the lowest T_{ni} in the simulation under the same N_D. Such difference between experimental and

simulation results may be due to following reasons: (1) the trimers in the simulation are monodisperse, while the LC oligomers in the experiment are polydisperse, (2) the degree of flexibility of the spacer between simulation and experiment is not the same, and (3) mainly because only entropic effects are considered in the simulations (*i.e.*, absence of π-π interactions and crystallinity). We attempted to add interactions between different components by changing the ε_{LJ} value of eq. S1 between mesogen, linker and extender beads, and favoring mesogen-to-mesogen attractions over the other interactions. However, we observed that it is a challenge to determine the T_{ni} when there is phase-separation (hence, confinement), occurring simultaneously. Both effects are beyond the scope of this study and to model this system would require systematic coarse-graining approaches,[85] like for example, using atomistic MD simulations as a reference to obtain a coarse-grained force-field.

The $T_{ni,oligomer}/T_{ni,monomer}$ of LC oligomers is greatly influenced when the spacer of LC monomer is short. In other words, the rate of T_{ni} change is much greater when shorter methylene spacers are introduced in the LC monomer (See Figure 6a). We also observed a similar tendency in the simulations (See Figure 6b). The simulations showed a sudden drop of the value of T_{ni} relative to the monomer for the system with N_L=1 and N_D=1. We hypothesize that the extender connected on the junction point serves as a defect on the LC ordering, and we observed that its effect on the value of T_{ni} is amplified if N_L is short. The effect of the extender on T_{ni} decreases as the length of the spacer increases. We attribute this behavior to the decrease in anisotropy of the LC oligomers as either N_L or N_D increases.

To verify our claim that the spacer and chain extender disrupt the ordering of mesogens and changes the shape anisotropy of the LC oligomers, we therefore obtain the shape anisotropy, $\langle\kappa^2\rangle$, which is calculated from the principal moments of the gyration tensor of the position vectors of the beads of a LC monomer or trimer. [86] In Figure 7, $\langle\kappa^2\rangle$ is calculated for the LC monomer (Figure 7a) and trimers (Figure 7b-d) at various temperatures near the vicinity of T_{ni}. The *x*-axis in Figure 7 is plotted in terms of $T-T_{ni}$ to facilitate comparison among different combinations of N_L and N_D. The brackets in $\langle\kappa^2\rangle$ refer to ensemble average in time and in number of LC oligomers. Note that $\langle\kappa^2\rangle$ is always greater when the temperature of the system is lower than T_{ni}. For the monomers (Figure 7a), the value of $\langle\kappa^2\rangle$ is high (indicating that the monomers are nearly rod-like where $\langle\kappa^2\rangle$=1 for a

line), and similar to the behavior of T_{ni}, where $\langle \kappa^2 \rangle$ decreases as N_L increases. For trimers, an increase in N_D at constant N_L or an increase in N_L at constant N_D decreases $\langle \kappa^2 \rangle$ which correlates with the decrease in T_{ni}.

Table 2. Summary of nematic-isortropic temperature of coarse-grained models of monomers and trimers from CG-MD simulations.

N_L	Monomers	Trimers			
		N_D=0	N_D=1	N_D=2	N_D=3
0	1.35 ± 0.01	--	--	--	--
1	0.99 ± 0.01	0.98 ± 0.01 (0.99)	0.92 ± 0.01 (0.93)	0.90 ± 0.01 (0.91)	0.86 ± 0.01 (0.87)
2	0.86 ± 0.01	0.83 ± 0.01 (0.96)	0.82 ± 0.01 (0.95)	0.80 ± 0.01 (0.93)	0.76 ± 0.01 (0.88)
3	0.77 ± 0.01	0.75 ± 0.01 (0.97)	0.74 ± 0.01 (0.96)	0.73 ± 0.01 (0.95)	0.72 ± 0.01 (0.94)

[a]The values in the parenthesis indicate the ratio of $T_{ni,oligomer}/T_{ni,monomer}$.

Table 3. Summary of nematic-isotropic temperatures of LC monomers and LC oligomers.

Spacer length (n) of LC monomer	T_{ni} of LC Monomer (ºC)[a]	T_{ni} of LC oligomer (ºC)[a]			
		m = 3	m = 5	m = 7	m = 9
3	128	80 (0.62)[b]	68 (0.53)	60 (0.47)	52 (0.40)
6	120	103 (0.86)	99 (0.83)	88 (0.73)	84 (0.70)
11	105	100 (0.96)	93 (0.89)	88 (0.85)	85 (0.82)

[a]T_{ni} is determined by POM while cooling from the isotropic phase.

[b]The values in the parenthesis indicate the ratio of $T_{ni,oligomer}/T_{ni,monomer}$.

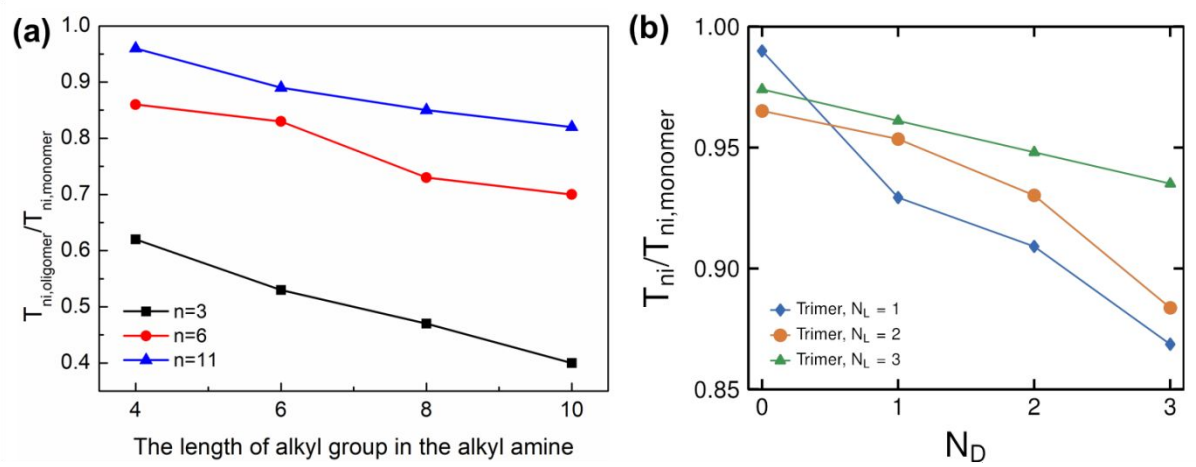

Figure 6. Rate of T_{ni} changes for LC oligomers. (a) Experimental and (b) simulation results.

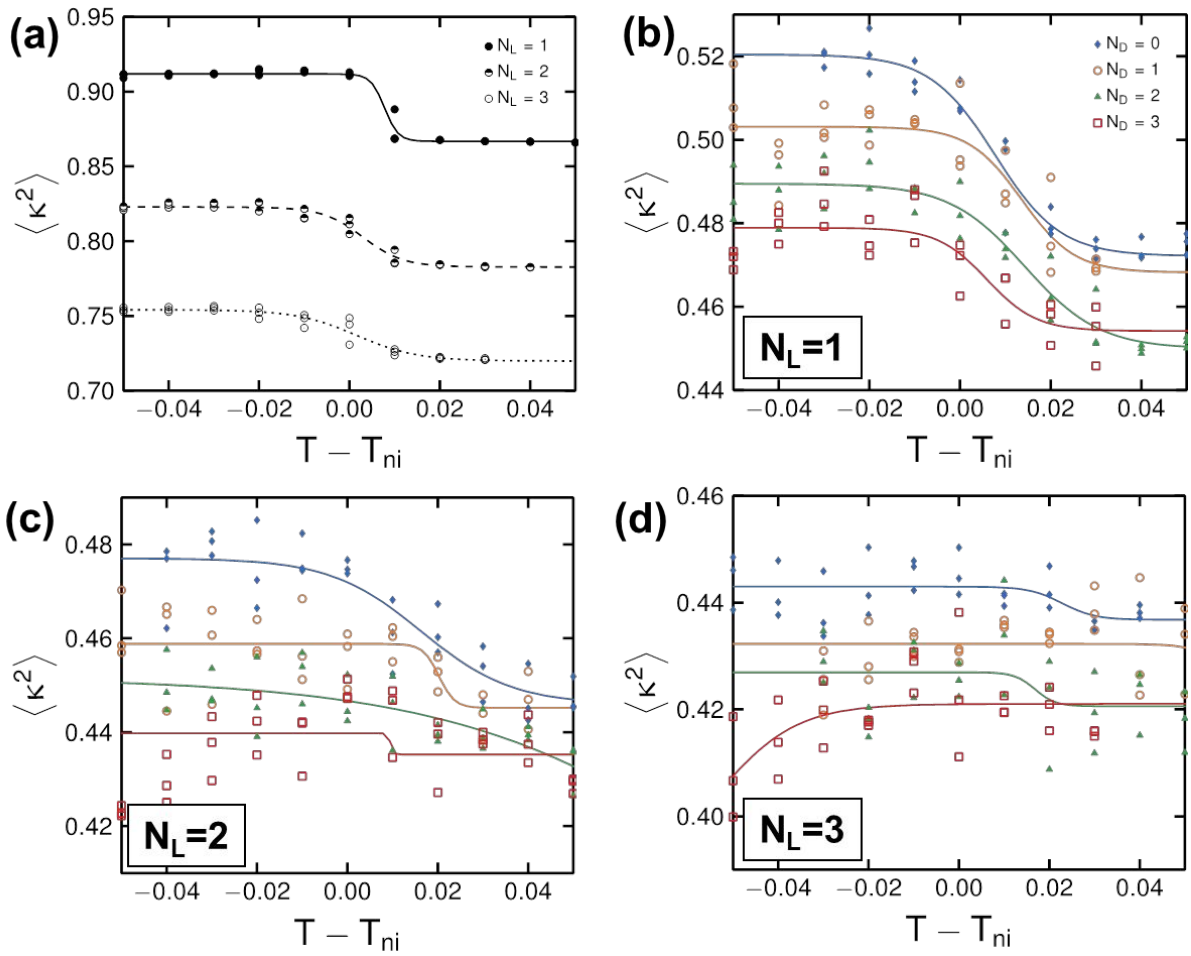

Figure 7. Shape anisotropy $\langle \kappa^2 \rangle$ of LC monomers and LC oligomers at different temperature. (a) LC monomer, (b) LC oligomers with N_L=1, (c) LC oligomers with N_L=2 and (d) LC oligomers with N_L=3. (Lines are guide to the eye.)

To gain further insight into the effect of N_L and N_D on the packing of mesogens in trimers, we investigated the systems at an isotropic temperature (T=1.10). Here we gauged the probability of how mesogens would pack, *e.g.*, whether it would be more of an intra-chain or an inter-chain packing. In Figure 8, we explored the probability of a mesogen to be in contact with another mesogen belonging to the same trimer through $g_{intra}(r)$, which represents the intra-chain contribution to the LC center-to-center radial distribution function, g(r), or contacts of an LC subunit within the trimer. Figure 8 shows that the lower value of N_L, g(r) has a higher proportion to intra-chain contacts (decreasing peak as you move from (a) to (c) in Figure 8). However, at constant N_L, the peak in $g_{intra}(r)$ is lower for lower N_D. These observations suggest that N_D promotes more intra-chain contacts, while N_L frustrates intra-chain contacts. The magnitude of change of $g_{intra}(r)$ is greater for N_L=1 as N_D is changed as opposed to N_L=3 (see blue arrows in Figure 8), suggesting that intra-chain packing in N_L=1 is more affected when N_D is changed. This is consistent with the observation that T_{ni} of the oligomer with N_L=1 decreases more relative to T_{ni} of the monomer than that of the oligomer with N_L=3, and is consistent with the trends for $T_{ni}/T_{ni,monomer}$ shown in Figure 6. Furthermore in Figure S8, we calculated the intra-chain correlation function at the T_{ni} and 0.5 below the T_{ni} and we observe similar trends in $g_{intra}(r)$ to the high temperature systems but the correlation peaks at the lower temperatures have higher intensities reflecting the better packing of mesogens in the nematic phase. The qualitatively similar behavior of $g_{intra}(r)$ in the isotropic and nematic phases is expected since all the simulations were pre-equilibrated at a temperature of T=1.0, which is above the T_{ni}.

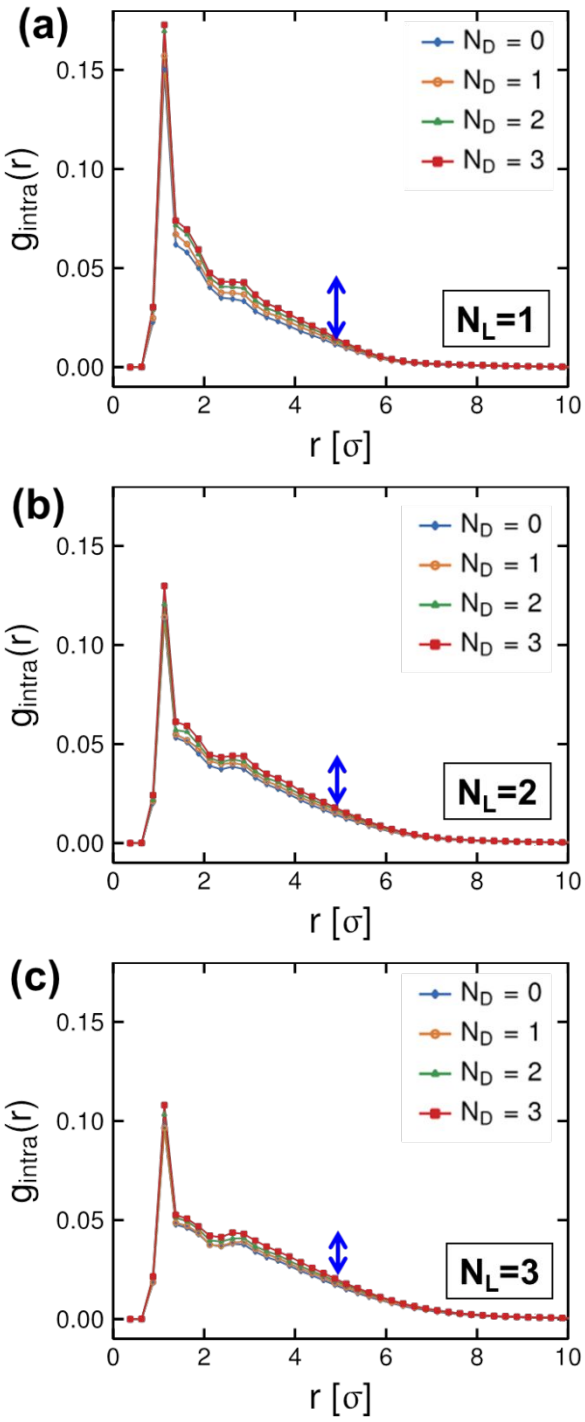

Figure 8. Probability of intrachain contacts, $g_{intra}(r)$ between mesogens in trimers having different values of N_L and N_D at T=1.10. (a) N_L = 1, (b) N_L = 2 and (c) N_L = 3.

Figure 9 summarizes the relationship between molecular structure of LC oligomers and the change in shape anisotropy based on the results from experiment and CG-MD simulation. First, the extension of a LC monomer to trimer (or a LC oligomer) by the introduction of chain extenders decreases the aspect ratio (as measured by its shape anisotropy, $\langle \kappa^2 \rangle$) and results in a decrease in T_{ni} (Figure 9a). Second, an increase in the chain extender length of the trimer (or the LC oligomer) decreases the aspect ratio and results in a decrease in T_{ni} (Figure 9b). Lastly, if the trimer (or the LC oligomer) is prepared by a LC monomer having shorter flexible spacer, the change (delta) of the aspect ratio is more significant, resulting in a considerable drop of T_{ni}, when comparing to the LC monomer having longer spacer (Figure 9c). According to the CG-MD results, these relationships between T_{ni} and the molecular structure of LC oligomers are mainly due to the difference in shape anisotropy of the LC oligomers upon change in their molecular parameters.

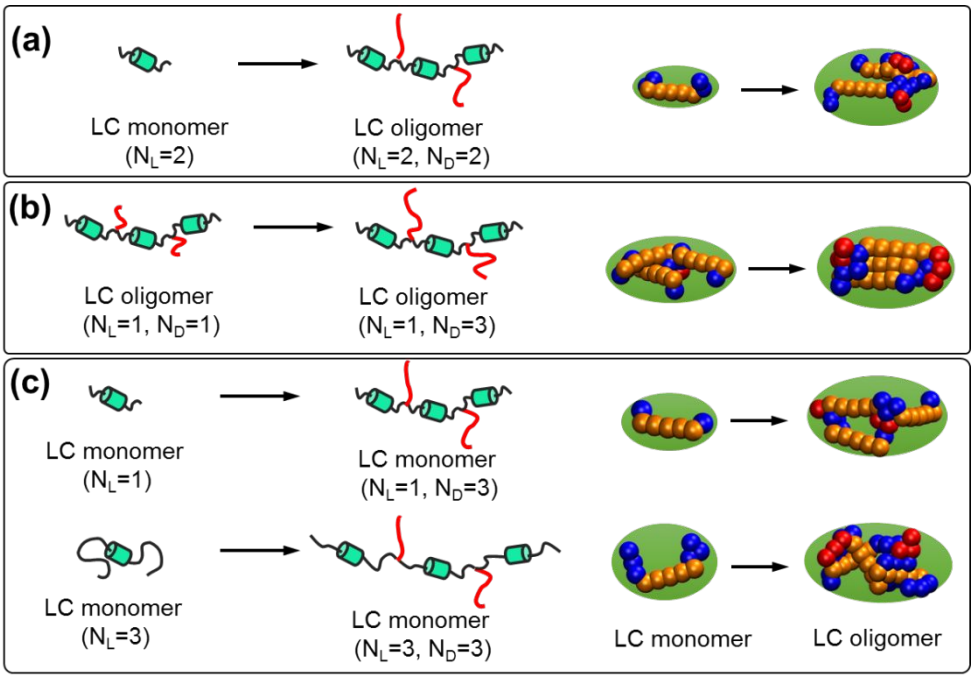

Figure 9. Proposed mechanism of change in shape anisotropy of LC oligomers. (a) Effect of chain extender, (b) effect of chain extender length, and (c) effect of spacer length in the LC monomer.

CONCLUSIONS

Our investigation in the synthesis, characterization and CG-MD simulation of model LC oligomers provides molecular insight into the effect of chain spacers and chain extenders on the ordering of LC oligomers. Specifically, we examined the effects of the length of the flexible spacer and alkyl chain extender on T_{ni} at which most dramatic change in the order parameter occurs. The results on the molecular-structure property relationships reveal that T_{ni} of LC oligomers gradually decreases with increasing the length of chain extender which is the non-mesogenic moiety. Interestingly, the decrease of T_{ni} in LC oligomers accelerates when the spacer length of LC oligomers is short. Based on the CG-MD results, we infer that such changes in T_{ni} is primarily resulted from the change in shape anisotropy of LC oligomers and is dependent on the molecular structure, which affects the packing behavior of constituent mesogens. Since the length of the flexible spacer and chain-extenders can bring a considerable impact on the resulting phase behaviors,[87-90] microstructures,[91-93] and even shape memory and actuation properties[91,94] of LC polymers and elastomers, our findings on the molecular-structure property relationships may offer useful guidelines to design LC oligomers and tailor their properties targeting molecularly-engineered shape changing materials.

ASSOCIATED CONTENT

Supporting Information

The Supporting Information is available free of charge on the ACS Publications website at DOI: XX.

^{1}H NMR spectra of LC monomer and LC oligomers, DSC traces of LC monomers, POM images of smectic and crystalline textures, thermal properties of LC monomers and LC oligomers, and details for the coarse-grained simulations.

AUTHOR INFORMATION

Corresponding Author

*Email: skahn@pusan.ac.kr

*Email: carrillojy@ornl.gov

ORCID

Suk-kyun Ahn: 0000-0002-6841-4213

Jan-Michael Carrillo: 0000-0001-8774-697X

Bobby G. Sumpter: 0000-0001-6341-0355

Author Contributions

The manuscript was written through contributions of all authors. All authors have given approval to the final version of the manuscript.

Notes

The authors declare no competing financial interest.

Acknowledgement

This work was supported by Basic Science Research Program through the National Research Foundation of Korea (NRF) funded by the Ministry of Education (2016R1D1A3B03931932 and 2019R1C1C1006048). Y. Guo, J. Lee and J. Son acknowledge BK21PLUS Program for partial financial support. The authors are grateful to Timothy White and Kyungmin Lee for kind donation of LC monomer. S. Ahn is also thankful to Kyu Hyun for helpful discussions. The computational portion of this research was performed at the Center for Nanophase Materials Sciences, which is a US Department of Energy Office of Science User Facility. This research used resources of the Oak Ridge Leadership Computing Facility at the Oak Ridge National Laboratory, which is supported by the Office of Science of the U.S. Department of Energy under Contract No. DE-AC05-00OR22725.

Table of Contents Image (TOC)

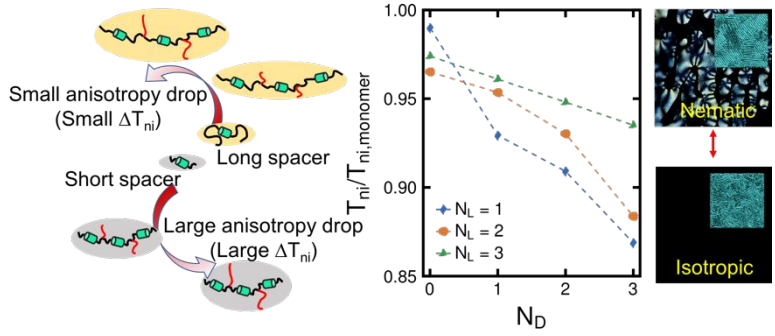

References

(1) White, T. J.; Broer, D. J. Programmable and adaptive mechanics with liquid crystal polymer networks and elastomers. *Nat. Mater.* **2015**, *14*, 1087-1098.

(2) Ohm, C.; Brehmer, M.; Zentel, R. Liquid crystalline elastomers as actuators and sensors. *Adv. Mater.* **2010**, *22*, 3366-3387.

(3) Kularatne, R. S.; Kim, H.; Boothby, J. M.; Ware, T. H. Liquid crystal elastomer actuators: synthesis, alignment, and applications. *J. Polym. Sci. Part B: Polym. Phys.* **2017**, *55*, 395-411.

(4) Liu, D.; Broer, D. J. Liquid crystal polymer networks: switchable surface topographies. *Liq. Cryst. Rev.* **2013**, *1*, 20-28.

(5) Kowalski, B. A.; Guin, T. C.; Auguste, A. D.; Godman, N. P.; White, T. J. Pixelated polymers: directed self assembly of liquid crystalline polymer networks. *ACS Macro Lett.* **2017**, *6*, 436-441.

(6) Liu, D.; Broer, D. J. Liquid crystal polymer networks: preparation, properties, and applications of films with patterned molecular alignment. *Langmuir* **2014**, *30*, 13499-13509.

(7) de Haan, L. T.; Schenning, A. P. H. J.; Broer, D. J. Programmed morphing of liquid crystal networks. *Polymer* **2014**, *55*, 5885-5896.

(8) Ware, T. H.; McConney, M. E.; Wie, J. J.; Tondiglia, V. P.; White, T. J. Voxelated liquid crystal elastomers. *Science* **2015**, *347*, 982-984.

(9) Schuhladen, S.; Preller, F.; Rix, R.; Petsch, S.; Zentel, R.; Zappe, H. Iris-like tunable aperture employing liquid-crystal elastomers. *Adv. Mater.* **2014**, *26*, 7247-7251.

(10) Yoon, H.-H.; Kim, D.-Y.; Jeong, K.-U.; Ahn, S.-k. Surface aligned main-chain liquid crystalline elastomers: tailored properties by the choice of amine chain extenders. *Macromolecules* **2018**, *51*, 1141-1149.

(11) Küpfer, J.; Finkelmann, H. Nematic liquid single crystal elastomers. *Die Makromol. Chemie, Rapid Commun.* **1991**, *12*, 717-726.

(12) Wermter, H.; Finkelmann, H. Liquid crystalline elastomers as artificial muscles. *e-Polym.* **2001**, *1*, 1-13.

(13) Camacho-Lopez, M.; Finkelmann, H.; Palffy-Muhoray, P.; Shelley, M. Fast liquid-crystal elastomer swims into the dark. *Nat. Mater.* **2004**, *3*, 307-310.

(14) Agrawal, A.; Yun, T.; Pesek, S. L.; Chapman, W. G.; Verduzco, R. Shape-responsive liquid crystal elastomer bilayers. *Soft Matter* **2014**, *10*, 1411-1415.

(15) Yang, H.; Buguin, A.; Taulemesse, J.-M.; Kaneko, K.; Méry, S.; Bergeret, A.; Keller, P. Micron-sized main-chain liquid crystalline elastomer actuators with ultralarge amplitude contractions. *J. Am. Chem. Soc.* **2009**, *131*, 15000-15004.

(16) Ohm, C.; Fleischmann, E.-K.; Kraus, I.; Serra, C.; Zentel, R. Control of the properties of micrometer-sized actuators from liquid crystalline elastomers prepared in a microfluidic setup. *Adv. Funct. Mater.* **2010**, *20*, 4314-4322.

(17) Yang, H.; Ye, G.; Wang, X.; Keller, P. Micron-sized liquid crystalline elastomer actuators. *Soft Matter* **2011**, *7*, 815-823.

(18) Fleischmann, E.-K.; Liang, H.-L.; Kapernaum, N.; Giesselmann, F.; Lagerwall, J.; Zentel, R. One-piece micropumps from liquid crystalline core-shell particles. *Nat. Commun.* **2012**, *3*, 1178.

(19) Fleischmann, E.-K.; Forst, F. R.; Koder, K.; Kapernaum, N.; Zentel, R. Microactuators from a main-chain liquid crystalline elastomer via thiol-ene "click" chemistry. *J. Mater. Chem. C* **2013**, *1*, 5885-5891.

(20) Lv, J.-a.; Liu, Y.; Wei, J.; Chen, E.; Qin, L.; Yu, Y. Photocontrol of fluid slugs in liquid crystal polymer microactuators. *Nature* **2016**, *537*, 179-184.

(21) Elias, A. L.; Harris, K. D.; Bastiaansen, C. W. M.; Broer, D. J.; Brett, M. J. Photopatterned liquid crystalline polymers for microactuators. *J. Mater. Chem.* **2006**, *16*, 2903-2912.

(22) Ohm, C.; Serra, C.; Zentel, R. A continuous flow synthesis of micrometer-sized actuators from liquid crystalline elastomers. *Adv. Mater.* **2009**, *21*, 4859-4862.

(23) van Oosten, C. L.; Bastiaansen, C. W. M.; Broer, D. J. Printed artificial cilia from liquid-crystal network actuators modularly driven by light. *Nat. Mater.* **2009**, *8*, 677-682.

(24) Sánchez-Ferrer, A.; Fischl, T.; Stubenrauch, M.; Albrecht, A.; Wurmus, H.; Hoffmann, M.; Finkelmann, H. Liquid-crystalline elastomer microvalve for microfluidics. *Adv. Mater.* **2011**, *23*, 4526-4530.

(25) Yan, Z.; Ji, X.; Wu, W.; Wei, J.; Yu, Y. Light-switchable behavior of a microarray of azobenzene liquid crystal polymer induced by photodeformation. *Macromol. Rapid Commun.* **2012**, *33*, 1362-1367.

(26) Torras, N.; Zinoviev, K. E.; Esteve, J.; Sanchez-Ferrer, A. Liquid-crystalline elastomer micropillar array for haptic actuation. *J. Mater. Chem. C* **2013**, *1*, 5183-5190.

(27) Wu, Z. L.; Buguin, A.; Yang, H.; Taulemesse, J.-M.; Le Moigne, N.; Bergeret, A.; Wang, X.; Keller, P. Microstructured nematic liquid crystalline elastomer surfaces with switchable wetting properties. *Adv. Funct. Mater.* **2013**, *23*, 3070-3076.

(28) Liu, X.; Wei, R.; Hoang, P. T.; Wang, X.; Liu, T.; Keller, P. Reversible and rapid laser actuation of liquid crystalline elastomer micropillars with inclusion of gold nanoparticles. *Adv. Funct. Mater.* **2015**, *25*, 3022-3032.

(29) Wu, Z. L.; Wang, Z. J.; Keller, P.; Zheng, Q. Light responsive microstructured surfaces of liquid crystalline network with shape memory and tunable wetting behaviors. *Macromol. Rapid Commun.* **2016**, *37*, 311-317.

(30) Zhan, Y.; Zhao, J.; Liu, W.; Yang, B.; Wei, J.; Yu, Y. Biomimetic submicroarrayed cross-linked liquid crystal polymer films with different wettability via colloidal lithography. *ACS Appl. Mater. Interfaces* **2015**, *7*, 25522-25528.

(31) Zhao, H.; Wie, J. J.; Copic, D.; Oliver, C. R.; Orbaek White, A.; Kim, S.; Hart, A. J. High-fidelity replica molding of glassy liquid crystalline polymer microstructures. *ACS Appl. Mater. Interfaces* **2016**, *8*, 8110-8117.

(32) Buguin, A.; Li, M.-H.; Silberzan, P.; Ladoux, B.; Keller, P. Micro-actuators: when artificial muscles made of nematic liquid crystal elastomers meet soft lithography. *J. Am. Chem. Soc.* **2006**, *128*, 1088-1089.

(33) Wang, Z.; Tian, H.; He, Q.; Cai, S. Reprogrammable, reprocessible, and self-healable liquid crystal elastomer with exchangeable disulfide bonds. *ACS Appl. Mater. Interfaces* **2017**, *9*, 33119-33128.

(34) Liu, D.; Broer, D. J. Self-assembled dynamic 3D fingerprints in liquid-crystal coatings towards controllable friction and adhesion. *Angew. Chem. Int. Ed.* **2014**, *53*, 4542-4546.

(35) Babakhanova, G.; Turiv, T.; Guo, Y.; Hendrikx, M.; Wei, Q.-H.; Schenning, A. P. H. J.; Broer, D. J.; Lavrentovich, O. D. Liquid crystal elastomer coatings with programmed response of surface profile. *Nat. Commun.* **2018**, *9*, 456.

(36) Liu, D.; Bastiaansen, C. W. M.; den Toonder, J. M. J.; Broer, D. J. Photo-switchable surface topologies in chiral nematic coatings. *Angew. Chem. Int. Ed.* **2012**, *51*, 892-896.

(37) Liu, D.; Broer, D. J. Light controlled friction at a liquid crystal polymer coating with switchable patterning. *Soft Matter* **2014**, *10*, 7952-7958.

(38) Liu, D.; Broer, D. J. New insights into photoactivated volume generation boost surface morphing in liquid crystal coatings. *Nat. Commun.* **2015**, *6*, 8334.

(39) Liu, D.; Liu, L.; Onck, P. R.; Broer, D. J. Reverse switching of surface roughness in a self-organized polydomain liquid crystal coating. *Proc. Natl. Acad. Sci. U.S.A.* **2015**, *112*, 3880-3885.

(40) Yang, Z.; Herd, G. A.; Clarke, S. M.; Tajbakhsh, A. R.; Terentjev, E. M.; Huck, W. T. S. Thermal and UV shape shifting of surface topography. *J. Am. Chem. Soc.* **2006**, *128*, 1074-1075.

(41) Agrawal, A.; Luchette, P.; Palffy-Muhoray, P.; Biswal, S. L.; Chapman, W. G.; Verduzco, R. Surface wrinkling in liquid crystal elastomers. *Soft Matter* **2012**, *8*, 7138-7142.

(42) Finkelmann, H.; Kock, H.-J.; Rehage, G. Investigations on liquid crystalline polysiloxanes 3. Liquid crystalline elastomers - a new type of liquid crystalline material. *Die Makromol. Chemie, Rapid Commun.* **1981**, *2*, 317-322.

(43) Sánchez-Ferrer, A.; Finkelmann, H. Thermal and mechanical properties of new main-chain liquid-crystalline elastomers. *Solid State Sci.* **2010**, *12*, 1849-1852.

(44) Donnio, B.; Wermter, H.; Finkelmann, H. A simple and versatile synthetic route for the preparation of main-chain, liquid-crystalline elastomers. *Macromolecules* **2000**, *33*, 7724-7729.

(45) Rousseau, I. A.; Mather, P. T. Shape memory effect exhibited by smectic-C liquid crystalline elastomers. *J. Am. Chem. Soc.* **2003**, *125*, 15300-15301.

(46) Burke, K. A.; Mather, P. T. Soft shape memory in main-chain liquid crystalline elastomers. *J. Mater. Chem.* **2010**, *20*, 3449-3457.

(47) Ware, T. H.; White, T. J. Programmed liquid crystal elastomers with tunable actuation strain. *Polym. Chem.* **2015**, *6*, 4835-4844.

(48) Ahn, S.-k.; Ware, T. H.; Lee, K. M.; Tondiglia, V. P.; White, T. J. Photoinduced topographical feature development in blueprinted azobenzene-functionalized liquid crystalline elastomers. *Adv. Funct. Mater.* **2016**, *26*, 5819-5826.

(49) Torbati, A. H.; Mather, P. T. A hydrogel-forming liquid crystalline elastomer exhibiting soft shape memory. *J. Polym. Sci. Part B: Polym. Phys.* **2016**, *54*, 38-52.

(50) Xia, Y.; Zhang, X.; Yang, S. Instant locking of molecular ordering in liquid crystal elastomers by oxygen-mediated thiol–acrylate click reactions. *Angew. Chem. Int. Ed.* **2018**, *57*, 5665-5668.

(51) Kim, H.; Boothby, J. M.; Ramachandran, S.; Lee, C. D.; Ware, T. H. Shape-changing materials: crystallized liquid crystal elastomers. *Macromolecules* **2017**, *50*, 4267-4275.

(52) Saed, M. O.; Ambulo, C. P.; Kim, H.; De, R.; Raval, V.; Searles, K.; Siddiqui, D. A.; Cue, J. M. O.; Stefan, M. C.; Shankar, M. R.; Ware, T. H. Molecularly-engineered, 4D-printed liquid crystal elastomer actuators. *Adv. Funct. Mater.* **2019**, *29*, 1806412.

(53) Ware, T. H.; Perry, Z. P.; Middleton, C. M.; Iacono, S. T.; White, T. J. Programmable liquid crystal elastomers prepared by thiol–ene photopolymerization. *ACS Macro Lett.* **2015**, *4*, 942-946.

(54) Yakacki, C. M.; Saed, M.; Nair, D. P.; Gong, T.; Reed, S. M.; Bowman, C. N. Tailorable and programmable liquid-crystalline elastomers using a two-stage thiol-acrylate reaction. *RSC Adv.* **2015**, *5*, 18997-19001.

(55) Saed, M. O.; Volpe, R. H.; Traugutt, N. A.; Visvanathan, R.; Clark, N. A.; Yakacki, C. M. High strain actuation liquid crystal elastomers via modulation of mesophase structure. *Soft Matter* **2017**, *13*, 7537-7547.

(56) McBride, M. K.; Martinez, A. M.; Cox, L.; Alim, M.; Childress, K.; Beiswinger, M.; Podgorski, M.; Worrell, B. T.; Killgore, J.; Bowman, C. N. A readily programmable, fully reversible shape-switching material. *Sci. Adv.* **2018**, *4*, eaat4634.

(57) Gelebart, A. H.; Mc Bride, M.; Schenning, A. P. H. J.; Bowman, C. N.; Broer, D. J. Photoresponsive fiber array: toward mimicking the collective motion of cilia for transport applications. *Adv. Funct. Mater.* **2016**, *26*, 5322-5327.

(58) Li, Y.; Hamed, S.; Geoffrey, R.; Che, Z.; Pengxiang, S.; Boxin, Z. Programmable 3D shape changes in liquid crystal polymer networks of uniaxial orientation. *Adv. Funct. Mater.* **2018**, *28*, 1802809.

(59) Hanzon, D. W.; Traugutt, N. A.; McBride, M. K.; Bowman, C. N.; Yakacki, C. M.; Yu, K. Adaptable liquid crystal elastomers with transesterification-based bond exchange reactions. *Soft Matter* **2018**, *14*, 951-960.

(60) Zhu, B.; Barnes, M. G.; Kim, H.; Yuan, M.; Ardebili, H.; Verduzco, R. Molecular engineering of step-growth liquid crystal elastomers. *Sens. Actuators B: Chem.* **2017**, *244*, 433-440.

(61) Pei, Z.; Yang, Y.; Chen, Q.; Terentjev, E. M.; Wei, Y.; Ji, Y. Mouldable liquid-crystalline elastomer actuators with exchangeable covalent bonds. *Nat. Mater.* **2014**, *13*, 36-41.

(62) Godman, N. P.; Kowalski, B. A.; Auguste, A. D.; Koerner, H.; White, T. J. Synthesis of elastomeric liquid crystalline polymer networks via chain transfer. *ACS Macro Lett.* **2017**, *6*, 1290-1295.

(63) Niu, H.; Wang, Y.; Wang, J.; Yang, W.; Dong, Y.; Bi, M.; Zhang, J.; Xu, J.; Bi, S.; Wang, B.; Gao, Y.; Li, C.; Zhang, J. Reducing the actuation threshold by incorporating a nonliquid crystal chain into a liquid crystal elastomer. *RSC Adv.* **2018**, *8*, 4857-4866.

(64) Ambulo, C.; Burroughs, J. J.; Boothby, J. M.; Kim, H.; Shankar, M. R.; Ware, T. H. 4D printing of liquid crystal elastomers. *ACS Appl. Mater. Interfaces* **2017**, *9*, 37332-37339.

(65) Kotikian, A.; Truby, R. L.; Boley, J. W.; White, T. J.; Lewis, J. A. 3D printing of liquid crystal elastomeric actuators with spatially programed nematic order. *Adv. Mater.* **2018**, *30*, 1706164.

(66) López-Valdeolivas, M.; Liu, D.; Broer, D. J.; Sánchez-Somolinos, C. 4D printed actuators with soft-robotic functions. *Macromol. Rapid Commun.* **2018**, *39*, 1700710.

(67) Lebwohl, P. A.; Lasher, G. Nematic-liquid-crystal order - a Monte Carlo calculation. *Phys. Rev. A* **1972**, *6*, 426-429.

(68) Berardi, R.; Fava, C.; Zannoni, C. A Gay–Berne potential for dissimilar biaxial particles. *Chem. Phys. Lett.* **1998**, *297*, 8-14.

(69) Care, C. M.; Cleaver, D. J. Computer simulation of liquid crystals. *Rep. Prog. Phys.* **2005**, *68*, 2665-2700.

(70) Berardi, R.; Muccioli, L.; Zannoni, C. Field response and switching times in biaxial nematics. *J. Chem. Phys.* **2008**, *128*, 024905.

(71) Brown, W. M.; Petersen, M. K.; Plimpton, S. J.; Grest, G. S. Liquid crystal nanodroplets in solution. *J. Chem. Phys.* **2009**, *130*, 044901.

(72) Gimenez Pinto, V. Modeling Liquid Crystal Polymeric devices. Ph.D. Thesis, Kent State University, Ohio, US, 2014.

(73) Nguyen, T. D.; Carrillo, J.-M. Y.; Matheson, M. A.; Brown, W. M. Rupture mechanism of liquid crystal thin films realized by large-scale molecular simulations. *Nanoscale* **2014**, *6*, 3083-3096.

(74) Konya, A.; Gimenez-Pinto, V.; Selinger, R. L. B. Modeling defects, shape evolution, and programmed auto-origami in liquid crystal elastomers. *Front. Mater.* **2016**, *3*, 24.

(75) Allen, M. P. Molecular simulation of liquid crystals. *Mol. Phys.* **2019**, *117*, 2391-2417.

(76) Milchev, A.; Egorov, S. A.; Binder, K.; Nikoubashman, A. Nematic order in solutions of semiflexible polymers: Hairpins, elastic constants, and the nematic-smectic transition. *J. Chem. Phys.* **2018**, *149*, 174909.

(77) Tsourtou, F. D.; Skountzos, E. N.; Peroukidis, S. D.; Mavrantzas, V. G. Molecular simulation of the high temperature phase behaviour of α-unsubstituted sexithiophene. *Soft Matter* **2018**, *14*, 8253-8266.

(78) Peláez, J.; Wilson, M. Molecular orientational and dipolar correlation in the liquid crystal mixture E7: a molecular dynamics simulation study at a fully atomistic level. *Phys. Chem. Chem. Phys.* **2007**, *9*, 2968-2975.

(79) Carrillo, J.-M. Y.; Seibers, Z. D.; Kumar, R.; Matheson, M. A.; Ankner, J. F.; Goswami, M.; Bhaskaran-Nair, K.; Shelton, W. A.; Sumpter, B. G.; Kilbey II, S. M. Petascale simulations of the morphology and the molecular interface of bulk heterojunctions. *ACS Nano* **2016**, *10*, 7008-7022.

(80) Plimpton, S. Fast parallel algorithms for short-range molecular dynamics. *J. Comput. Phys.* **1995**, *117*, 1-19.

(81) Brown, W. M.; Wang, P.; Plimpton, S. J.; Tharrington, A. N. Implementing molecular dynamics on hybrid high performance computers – short range forces. *Comput. Phys. Commun.* **2011**, *182*, 898-911.

(82) Stevens, H.; Rehage, G.; Finkelmann, H. Phase transformations of liquid crystalline side-chain oligomers. *Macromolecules* **1984**, *17*, 851-856.

(83) Pugh, C.; Kiste A. L. Molecular engineering of side-chain liquid crystalline polymers by living polymerizations. *Prog. Polym. Sci.* **1997**, *22,* 601-691.

(84) Broer, D. J.; Mol, G. N.; Challa, G. In-situ photopolymerization of oriented liquid-crystalline acrylates, 5. Influence of the alkylene spacer on the properties of the mesogenic monomers and the formation and properties of oriented polymer networks. *Makromol. Chem.* **1991**, *192*, 59-74.

(85) Rühle, V.; Junghans, C.; Lukyanov, A.; Kremer, K.; Andrienko, D. Versatile object-oriented toolkit for coarse-graining applications. *J. Chem. Theory Comput.* **2009**, *5*, 3211-3223.

(86) Theodorou, D. N.; Suter, U. W. Shape of unperturbed linear polymers: polypropylene. *Macromolecules* **1985**, *18*, 1206-1214.

(87) Craig, A. A.; Imrie, C. T. Effect of spacer length on the thermal properties of side-chain liquid crystal polymethacrylates. 2. synthesis and characterization of the poly[.omega.-(4'-cyanobiphenyl-4-yloxy)alkyl methacrylate]s. *Macromolecules*, **1995**, *28*, 3617-3624.

(88) Chang, S.; Han, C. D. Effect of flexible spacer length on the phase transitions and mesophase structures of main-chain thermotropic liquid-crystalline polyesters having bulky pendent side groups. *Macromolecules*, **1997**, *30*, 1670-1684.

(89) Noirez, L.; Ungerank, M.; Stelzer, F. Dependence of the stereoregularity on the structure and the conformation of side-chain liquid crystalline polynorbornenes of various spacer lengths. *Macromolecules*, **2001**, *34*, 7885-7893.

(90) Ahn, S.-k.; Gopinadhan, M.; Deshmukh, P.; Lakhman, R. K.; Osuji, C. O.; Kasi, R. M. Cholesteric mesophase in side-chain liquid crystalline polymers: influence of mesogen interdigitation and motional decoupling. *Soft Matter* **2012**, *8*, 3185-3191.

(91) Ahn, S.-k.; Deshmukh, P.; Gopinadhan, M.; Osuji, C. O.; Kasi, R. M. Side-chain liquid crystalline polymer networks: exploiting nanoscale smectic polymorphism to design shape-memory polymers. *ACS Nano* **2011**, *5*, 3085-3095.

(92) Xie, H.-l.; Ni, B.; Liu, Q.; Wang, J.; Yang, S.; Zhang, H.-l.; Chen, E.-q. Self organization of main-chain/side-chain liquid crystalline polymer based on "jacketing" effect with different lengths of spacer: from smectic to hierarchically ordered structure. *RSC Adv.* **2015**, *5*, 97187-97194.

(93) Kim, H.; Zep, A.; Ryu, S. H.; Ahn, H.; Shin, T. J.; Lee, S. B.; Pociecha, D.; Gorecka, E.; Yoon, D. K. Linkage-length dependent structuring behaviour of bent-core molecules in helical nanostructures. *Soft Matter* **2016**, *12*, 3326-3330.

(94) Ahn, S.-k.; Kasi, R. M. Exploiting microphase-separated morphologies of side-chain liquid crystalline polymer networks for triple shape memory properties. *Adv. Funct. Mater.* **2011**, *21*, 4543-4549.